



## LJMU Research Online

**Sansalone, G, Profico, A, Wroe, S, Allen, K, Ledogar, J, Ledogar, S, Mitchell, DR, Mondanaro, A, Melchionna, M, Castiglione, S, Serio, C and Raia, P**

**Homo sapiens and Neanderthals share high cerebral cortex integration into adulthood**

<http://researchonline.ljmu.ac.uk/id/eprint/19024/>

### Article

**Citation** (please note it is advisable to refer to the publisher's version if you intend to cite from this work)

**Sansalone, G, Profico, A, Wroe, S, Allen, K, Ledogar, J, Ledogar, S, Mitchell, DR, Mondanaro, A, Melchionna, M, Castiglione, S, Serio, C and Raia, P (2023) Homo sapiens and Neanderthals share high cerebral cortex integration into adulthood. Nature Ecology and Evolution. 7 (1). pp. 42-50.**

LJMU has developed [LJMU Research Online](#) for users to access the research output of the University more effectively. Copyright © and Moral Rights for the papers on this site are retained by the individual authors and/or other copyright owners. Users may download and/or print one copy of any article(s) in LJMU Research Online to facilitate their private study or for non-commercial research. You may not engage in further distribution of the material or use it for any profit-making activities or any commercial gain.

The version presented here may differ from the published version or from the version of the record. Please see the repository URL above for details on accessing the published version and note that access may require a subscription.

For more information please contact [researchonline@ljmu.ac.uk](mailto:researchonline@ljmu.ac.uk)

<http://researchonline.ljmu.ac.uk/>

Figure #	Figure title One sentence only	Filename This should be the name the file is saved as when it is uploaded to our system. Please include the file extension. i.e.: <i>Smith_ED_Fig1.jpg</i>	Figure Legend If you are citing a reference for the first time in these legends, please include all new references in the main text Methods References section, and carry on the numbering from the main References section of the paper. If your paper does not have a Methods section, include all new references at the end of the main Reference list.
Extended Data Table 1	R-PLS values	Extended_Data_Table1.xlsx	R-PLS of separate PLS analyses performed on the different postnatal ontogenetic stages of <i>H. sapiens</i> , <i>P. troglodytes</i> , <i>G. gorilla</i> and <i>Pongo</i> species.
Extended Data Fig. 1	Endocast local integration assessment	Extended_Data_Fig1.tif	The set of each semilandmark (a) and its 9 closest semilandmarks define the N-Core (b). The remaining semilandmarks define the C-Core (c). The N-Core and R-Core are subjected to two independent GPAs and the covariation between the two-blocks is calculated by PLS (d). With CR the GPA is computed the entire set (e). The values from PLS and CR analyses are used to create a colour map of integration (f) and modularity (g).
Extended Data Table 2	Effect sizes of separate PLS analyses	Extended_Data_Table2.xlsx	Effect sizes of separate PLS analyses performed the different postnatal ontogenetic stages of <i>H. sapiens</i> , <i>P. troglodytes</i> , <i>G. gorilla</i> and <i>Pongo</i> when accounting for size effect.
Extended Data Fig. 2	Evolutionary rates of CR values within the Cercopitheciinae clade.	Extended_Data_Fig2.tiff	
Extended Data Fig. 3	Evolutionary rates of CR values within the Strepsirrhini.	Extended_Data_Fig3.tiff	
Extended Data Fig. 4	Evolutionary rates of CR values within the family Cebidae.	Extended_Data_Fig4.tiff	
Extended Data Table 3	CR values measured after size and phylogenetic correction.	Extended_Data_Table3.xlsx	

1

Item	Present?	Filename This should be the name the file is saved as when it is uploaded to our system, and should include the file extension. The extension must be .pdf	A brief, numerical description of file contents. i.e.: <i>Supplementary Figures 1-4, Supplementary Discussion, and Supplementary Tables 1-4.</i>
Supplementary Information	Yes	Supplementary_information.pdf	Supplementary Figures 1-4, Supplementary Tables 1-3 Supplementary methods; Specimens institutional codes; Tree in Newick format.
Reporting Summary	Yes	Sansalone_RS.pdf	

Peer Review Information	No	OFFICE USE ONLY
-------------------------	----	-----------------

2

Parent Figure or Table	Filename This should be the name the file is saved as when it is uploaded to our system, and should include the file extension. i.e.: <i>Smith_SourceData_Fig1.xls</i> , or <i>Smith_Unmodified_Gels_Fig1.pdf</i>	Data description i.e.: Unprocessed Western Blots and/or gels, Statistical Source Data, etc.
Source Data Fig. 1	Main_text_Figure1_SourceData.xlsx	Statistical Test Results and Display
Source Data Fig. 2	Main_text_Figure2_SourceData.xlsx	Statistical Test Results and Display
Source Data Fig. 3	Main_text_Figure3_SourceData.xlsx	Statistical Test Results and Display
Source Data Extended Data Table 1	Extended_Data_Table1_Source_Data.xlsx	Statistical Test Results
Source Data Extended Data Fig. 1	Not applicable	Methods Description - Artwork
Source Data Extended Data Table 2	Extended_Data_Table_Source_Data.xlsx	Statistical Test Results
Source Data Extended Data Fig. 2	Extended_Data_Figure2_SourceData.xlsx	Statistical Test Results and Display
Source Data Extended Data Fig. 3	Extended_Data_Figure3_SourceData.xlsx	Statistical Test Results and Display
Source Data Extended Data Fig. 4	Extended_Data_Figure4_SourceData.xlsx	Statistical Test Results and Display
Source Data Extended Data Table 3	Extended_Data_Table_Source_Data.xlsx	Statistical Test Results

3

## 4 **Homo sapiens and Neanderthals share high cerebral cortex integration into** 5 **adulthood**

6 **Authors:** Gabriele Sansalone<sup>1,2\*†</sup>, Antonio Profico<sup>3\*†</sup>, Stephen Wroe<sup>1</sup>, Kari Allen<sup>4</sup>, Justin  
7 Ledogar<sup>5</sup>, Sarah Ledogar<sup>1,6</sup>, Dave Rex Mitchell<sup>7</sup>, Alessandro Mondanaro<sup>8</sup>, Marina Melchionna<sup>9</sup>,  
8 Silvia Castiglione<sup>9</sup>, Carmela Serio<sup>10</sup>, Pasquale Raia<sup>9</sup>

9

10 **Affiliations:** <sup>1</sup>Function, Evolution & Anatomy Research Lab, Zoology Division, School of  
11 Environmental and Rural Science, University of New England, NSW, 2351, Armidale, Australia  
12 <sup>2</sup>Institute for Marine Biological Resources and Biotechnology (IRBIM), National Research Council,  
13 Messina 98122, Italy  
14 <sup>3</sup>Department of Biology, University of Pisa, Pisa, Italy Via Derna 1, 56126 Pisa (Italy)  
15 <sup>4</sup>Department of Neuroscience, Washington University School of Medicine, 660 S. Euclid Ave., St.  
16 Louis, MO 63110-1010, USA  
17 <sup>5</sup>Department of Health Sciences, East Tennessee State University, Johnson City, TN 37614  
18 <sup>6</sup>Department of Archaeology & Palaeoanthropology, School of Humanities, University of New  
19 England, NSW 2351, Armidale, Australia  
20 <sup>7</sup>College of Science and Engineering, Flinders University, 5042, Adelaide, SA, Australia

21 <sup>8</sup>Department of Earth Sciences, Università degli Studi di Firenze, Via G. La Pira 4, 50121 Firenze,  
22 Italy

23 <sup>9</sup>Department of Earth Sciences, Environment and Resources, Università degli Studi di Napoli  
24 Federico II, Via Cinthia 21, 80126, Monte Sant'Angelo, Naples, Italy

25 <sup>10</sup>Research Centre in Evolutionary Anthropology and Palaeoecology, School of Biological and  
26 Environmental Sciences, Liverpool John Moores University, Liverpool, England

27

28 \*Corresponding authors: gsansalone@uniroma3.it; antonio.profico@gmail.com

29 † These authors contributed equally

30

31 **Abstract:** There is controversy around the mechanisms that guided the change in brain shape  
32 during the evolution of modern humans. It has long been held that different cortical areas evolved  
33 independently from each other to develop their unique functional specializations. However, some  
34 recent studies suggest that high integration between different cortical areas could facilitate the  
35 emergence of equally extreme, highly specialized brain functions. Here, we analyze the evolution of  
36 brain shape in primates using 3D geometric morphometrics of endocasts. We aim to determine  
37 firstly, whether modern humans present unique developmental patterns of covariation between brain  
38 cortical areas and secondly, whether hominins experienced unusually high rates of evolution in  
39 brain covariation as compared to other primates. Based on analyses including modern humans and  
40 other extant great apes at different developmental stages, we first demonstrate that, unlike our  
41 closest living relatives, *Homo sapiens* retains high levels of covariation between cortical areas into  
42 adulthood. Among the other great apes, high levels of covariation are only found in immature  
43 individuals. Secondly, at the macroevolutionary level, our analysis of 400 endocasts, representing  
44 148 extant primate species and 6 fossil hominins, shows that strong covariation between different  
45 areas of the brain in *H. sapiens* and *Homo neanderthalensis* evolved under distinctly higher  
46 evolutionary rates than in any other primate, suggesting that natural selection favored a greatly  
47 integrated brain in both species. These results hold when extinct species are excluded and allometric  
48 effects are accounted for. Our findings demonstrate that high covariation in the brain may have  
49 played a critical role in the evolution of unique cognitive capacities and complex behaviors in both  
50 modern humans and Neanderthals.



51 **Introduction**

52  
53 The modern human brain is remarkable in its size, unusually globular shape, and extreme left-right  
54 asymmetry which are all thought to have contributed to the evolution of our exceptional cognitive  
55 capacities<sup>1-5</sup>. Historically, two main models have been invoked to explain the evolution of the brain:  
56 i) the ‘concerted’ model, assuming that developmental integration affects brain evolution globally  
57 and ii) the ‘mosaic’ model, that is the idea that functional units of the brain may co-evolve or evolve  
58 independently according to the distribution of selection pressures acting on them<sup>6-9</sup>. By deploying  
59 mosaicism, a brain module could be fine-tuned by selection to optimize specific tasks regardless of  
60 what happens in other areas of the brain<sup>10-14</sup>. Volumetric and morphometric analyses have  
61 demonstrated that selective expansion of discrete brain areas closely reflects the establishment of  
62 functional connections between them, enabling specific cognitive tasks<sup>14-16</sup>. It has also been  
63 proposed that mosaicism may have promoted behavioural flexibility and increased the ability to  
64 respond to changes in selective regimes<sup>13</sup>. However, the hypothesis of the brain modular evolution  
65 has been challenged by the recent observation that traits’ covariation can favour the rapid evolution  
66 of extreme, highly specialised morphotypes, provided that selection vectors align with major axes  
67 of phenotypic variation<sup>17,18</sup>. Within this ‘concerted’ framework, it has been argued that the multiple,  
68 high-level functional specialisations of the modern human brain could originate from selection for  
69 fine coordination between different brain units to shared functional ends, without effecting any  
70 major changes in the relative proportions of specific brain areas<sup>10,19,20</sup>. Despite their apparent  
71 polarisation the concerted and mosaic brain hypotheses are not mutually exclusive<sup>16</sup>. Mosaicism  
72 does not rule out co-variation between brain units, as long as this reflects a response to shared  
73 functional demands, and a concerted brain can be the result of an adaptive process rather than the  
74 product of developmental constraints<sup>21</sup>.

75 A key question regarding the uniqueness of the modern human brain is whether its evolution  
76 branched away from the developmental programme characterising our living relatives. Studying the  
77 developmental patterns of morphological concertedness (or integration) as opposed to mosaicism  
78 (or modularity) between human brain areas and comparing this pattern to those of other great apes  
79 would help us determine to what extent the organization of cortical areas in *Homo sapiens* may  
80 actually be remarkable<sup>1,22-25</sup>. Another important issue is to understand whether, at the macro-  
81 evolutionary scale, humans display higher evolutionary rates toward either brain modularity or  
82 integration. This would offer direct evidence of selection favouring the emergence of major changes  
83 in the patterns of co-variation between cortical areas.

84  
85 To address these questions, we have applied three dimensional geometric morphometrics to  
86 measure and visualise the relative magnitudes of morphological co-variation in primate virtual brain  
87 endocasts. Traditionally, investigations into patterns of covariation between different regions of the  
88 brain have relied on comparative volumetric analyses (i.e., of relative sizes) of brain subunits.  
89 However, volumetric comparisons are silent on the shape component (position and orientation) of  
90 brain form, which potentially captures aspects of brain evolution not predicted by size alone<sup>13</sup>.  
91 Furthermore, in contrast to volumetric data, shape data are comparatively rare for extinct species.  
92 Hence, studying patterns of covariation directly on cranial endocasts represents the single most  
93 informative means of gaining direct evidence on the evolutionary patterns of brain evolution across  
94 hominins (*Homo sapiens* and its extinct close relatives). To gain this insight, we have combined a  
95 phylogenetic comparative method based on phylogenetic ridge regression to determine the presence  
96 of shifts in the evolutionary rates across primate history with a novel strategy to measure and map  
97 phenotypic covariation on brain cortical areas. As brains do not fossilise, evidence of fossil species’  
98 brain evolution can be derived from the virtual fillings of the bony braincase - or endocasts - which  
99 can adequately approximate the outer brain morphology.

100 Our datasets comprise 127 postnatal virtual endocasts, sampled from the eruption of  
101 deciduous dentition through adulthood, for *H. sapiens*, *Pan troglodytes*, *Gorilla gorilla* and two

102 species of *Pongo* for the analysis of developmental patterns and, for the macroevolutionary study  
103 400 endocasts representing 154 extant and extinct species, including *Australopithecus africanus*,  
104 *Paranthropus boisei*, *Homo ergaster*, *Homo erectus*, *Homo heidelbergensis* and *H.*  
105 *neanderthalensis*. We explicitly tested whether i) specific patterns of modularity or integration  
106 between cortical areas can be identified through human brain development and how these relate to  
107 those of extant great apes; and ii) whether the hominin brain displays higher rates of evolution  
108 toward either increased integration or modularity.

## 109 Results

110 *Question 1. Does the human brain cortical covariation differ to that of other great apes?*

111 We performed separate partial least squares (PLS) analyses on 4 successive postnatal  
112 developmental stages of *Gorilla gorilla*, *Pan troglodytes* and *Homo sapiens*. We further included in  
113 the analysis *Pongo abelii* and *Pongo pygmaeus* (Fig. 1). Yet, given the paucity of available  
114 orangutan specimens we had to group them together and therefore did not explore covariation  
115 between individual brain modules in *Pongo*. The developmental stages were defined following  
116 refs.<sup>26,27</sup>: Stage 2 = all deciduous dentition fully erupted; Stage 3 = deciduous dentition and at least  
117 fully erupted M1; Stage 4 = M2 fully erupted; Adult = full permanent dentition. The PLS method  
118 allows the exploration of covariation patterns between different sets of shape variables (here brain  
119 subunits), whereas r-PLS (measured using the  $r^2$  derived from PLS analysis based on 999  
120 permutations, Methods and Extended Data Tables 1-2 and Extended Data Fig. 1) is the correlation  
121 coefficient and can be used as a measure of the magnitude of covariation.

122 Our results show that integration of the brain in *H. sapiens* and *P. troglodytes* is similar  
123 through the pre-adult stages (Stages 2 to 4; Fig. 1a and Extended Data Table 1). Yet, in  
124 chimpanzees (and in gorillas from stage 4 onwards), r-PLS significantly drops in adulthood,  
125 whereas in *H. sapiens* the brain remains significantly integrated into adulthood (Fig. 1 and Extended  
126 Data Table 1). The patterns of covariation between brain cortical modules are almost identical in  
127 adult *Pan* and *Gorilla* individuals, pointing to strong covariation between the occipital and  
128 temporal, and frontal and parietal modules, respectively (Fig. 1b). Comparable results are obtained  
129 when controlling for brain size (Extended Data Table 2), and whether *Pongo* species (grouped as  
130 one) are included. These results suggest that the shape covariation patterns observed during  
131 development are largely independent from allometric effects and that humans significantly depart  
132 from the brain developmental patterns shared by the other greater apes.

133 Using two-block PLS to measure the degree of association between different cortical areas we  
134 confirmed the proposition that the brain of *H. sapiens* retains high levels of morphological  
135 integration throughout growth, unlike other great apes (Fig. 1b,c). We applied for the first time a  
136 novel approach to map the magnitude of morphological integration (Methods and Extended Data  
137 Fig. 1) directly onto the endocast surface without defining any a priori module. This approach  
138 involves parcelling out the brain endocasts into small independent "modulets" centred around a  
139 single semilandmark and calculating the level of morphological integration of the modulets with the  
140 rest of the endocast. The average values of integration calculated at each semilandmark is  
141 subsequently used to create maps of integration intensity.

142 Charting the magnitude of integration over the endocasts at different developmental stages  
143 reveals clear differences between *H. sapiens* and *P. troglodytes* (Fig. 1a,c). At stage 2 the human  
144 brain displays high integration over the parietal and occipital regions. At stages 3 and 4 strong  
145 integration centres on the frontal and occipital lobes. In the adult stage (4) humans show the greatest  
146 level of integration over the parietal, temporal and prefrontal regions. Chimpanzees follow a  
147 different developmental pattern, showing poorly integrated frontal and parietal areas throughout  
148 postnatal growth and relatively stronger integration at the level of temporal and prefrontal areas.

149  
150  
151  
152

153 *Question 2. Did hominins evolve towards high cortical integration?*

154 We measured the covariation between four brain subunits (corresponding to frontal, parietal,  
155 temporal and occipital regions, see Methods and Extended Data Table 3) at the macroevolutionary  
156 level, by means of Covariance Ratio (CR; a measure of the overall covariation between modules  
157 divided by the overall covariation within modules, see Methods).

158 Our results show that hominoid (apes) brains are morphologically distinct in shape (Fig. 2a) and  
159 display higher levels of covariation between brain cortical areas (CR = 1.01 indicating high  
160 covariation, see Methods) than any other primate group (Fig. 2b, Methods and Extended Data Table  
161 2). Platyrrhini and Strepsirrhini display the lowest magnitude of covariation (CR = 0.76 and 0.72  
162 respectively) between brain modules, whereas Cercopithecinae and Colobinae fall in between  
163 hominoids and all other primates (CR = 0.83 and 0.91 respectively). Accounting for allometry did  
164 not alter the described pattern, suggesting that size has a limited impact on the brain covariation  
165 patterns observed at the macroevolutionary level (Extended Data Table 3).

166 In keeping with our ontogenetic analyses, we devised a novel approach to map the metrics for the  
167 magnitude of covariation, the CR, over the digital endocasts. These brain maps show that hominins  
168 are characterized by the highest evolutionary rates in CR (Fig. 2b). Great apes display higher values  
169 of covariation in the occipital and parieto-frontal regions and lower levels over the temporal areas.  
170 In contrast, lesser apes show lower covariation in the pre-frontal areas closer to the olfactory bulbs  
171 and over the temporal region (Fig. 2b).

172 Among Cercopithecinae, high evolutionary rates are recorded in Papionini (Fig. 2b and Extended  
173 Data Fig. 2). Conversely, Strepsirrhini (two-tailed  $p = 0.001$ ) are characterized by a rate slowdown,  
174 as were capuchin and squirrel monkeys (family Cebidae, two-tailed  $p = 0.002$ ) among New World  
175 monkeys (Fig. 2b and Extended Data Figs. 3-4). Mapping CR values over the endocast surfaces  
176 reveals different patterns in different primate clades. Cercopithecinae show higher integration in the  
177 occipital and frontal regions than elsewhere on the brain. Colobinae, Platyrrhini and Strepsirrhini  
178 display similar distribution of the CR values over the endocast, with the areas corresponding to the  
179 frontal and pre-frontal cortical areas and the temporal regions showing moderate covariation (Fig.  
180 2b).

181  
182 Within Hominoidea, *H. neanderthalensis* and *H. sapiens* show the highest rate of evolution of brain  
183 covariation (two tailed  $p = 1.00$ , Fig. 3). Interestingly, *A. africanus* was characterized by  
184 evolutionary rates comparable to those of *P. troglodytes* suggesting a graded trend for increased rate  
185 of CR evolution among hominins (Fig. 3a), leading to the highly integrated brain of *Homo*,  
186 especially evident in the parietal area (Fig. 3b).

187  
188  
189  
190  
191 **Discussion**

193 *Homo sapiens* and the other great apes share high covariation between different cortical areas of the  
194 brain throughout most postnatal development. However, only *Homo sapiens* retains such strong  
195 morphological integration into adulthood. This finding is consistent with other reports indicating  
196 that the cortical areas of the human brain are tightly integrated throughout the adult life<sup>12,28</sup>.

197 Connectome analysis suggests an evolutionary shift in the human brain to enhance global network  
198 integration over that of the chimpanzee<sup>29</sup>, indicating that humans evolved strong covariation even  
199 among spatially distant brain regions<sup>30</sup> (which is consistent with our Fig. 1c). This evolutionary  
200 pattern seems to have deep evolutionary roots. Hominins show a trend for an increased magnitude  
201 of covariation between different brain regions, escalating through Middle to Late Pleistocene  
202 human species (*H. sapiens* and *H. neanderthalensis*). This finding contradicts the common  
203 perception that functional specialisation in the modern human brain arises from a modular

204 architecture (e.g., semi-independent evolution of different cortical areas)<sup>13</sup>, but is in agreement with  
205 studies of encephalised non-mammalian vertebrates suggesting that high integration may drive  
206 functional specialisation in the brain, even among distantly related taxa and under very different  
207 selective scenarios<sup>31</sup>. Our findings similarly suggest that coordinated changes in brain shape may  
208 have played a major role in maintaining the functional association between brain subunits,  
209 ultimately leading to the derived cognitive specialisation observed in *Homo*.

210 Charting morphological integration over the endocasts shows that the great apes are clearly  
211 distinct from the lesser apes, suggesting that a shift in the spatial patterns of covariation (and not  
212 just in the magnitude of integration or relative brain size) occurred at the time of divergence  
213 between the two groups. Hominins show a high degree of covariation in the parietal and frontal  
214 regions, which are thought to have played a fundamental role in the evolution of cognitive  
215 capacities unique to humans<sup>32,33</sup>. Modifications in the parietal regions are thought to represent a  
216 derived condition apparent only within the most recent *Homo sapiens* populations<sup>23,34</sup>. The parietal  
217 cortex is involved in different association tasks such as dexterity, self-awareness and visual  
218 imaging<sup>35</sup>. These functions confer the capacity to translate cognition into novel behavioural  
219 attributes, allowing the incorporation of tools and technology into behavioural patterns<sup>33,36</sup>.

220 *Australopithecus africanus*, *H. ergaster* and *H. erectus* display evolutionary rates like, or  
221 slightly higher than those showed by *P. troglodytes* and *P. paniscus* (Fig. 3a). In general, larger-  
222 bodied species, mostly occurring among hominoids and papionins, are marked by higher rates of  
223 covariation among brain areas<sup>37</sup>. Yet, even after correcting for brain size, the *Homo* clade still  
224 shows the highest levels and rates of brain cortex covariation (Extended Data Table 3). This  
225 suggests that the major shift in the pattern of brain shape covariation emerged independently from  
226 size and, likely, occurred within these species only. This increased level of interconnection between  
227 different cortical areas of the brain may have facilitated the emergence of derived cognitive  
228 capacities in Neanderthals as suggested by the palaeoanthropological record<sup>38-41</sup>. However, modern  
229 humans and Neanderthals have distinctly different brain morphologies, suggesting that high levels  
230 of covariation might have been inherited from their last common ancestor and that brain shape  
231 evolution then followed divergent trajectories in *H. neanderthalensis* and *H. sapiens*<sup>42</sup>. This  
232 evidence brings into question the role of globularity in the emergence of high cognitive abilities in  
233 *Homo sapiens*. Neanderthals, and the other great apes, did not go through a “globularisation phase”  
234 during the earliest postnatal growth stages, retaining the plesiomorphic, antero-posteriorly elongated  
235 adult brain common to archaic *Homo* species<sup>43,44</sup>. The development of a globular brain is exclusive  
236 to modern humans<sup>45</sup> and its role in maintaining high levels of integration into adulthood deserves  
237 further investigation.

238 Our findings do not favour either the mosaic or the concerted model of brain evolution,  
239 suggesting that the debate between these two hypotheses of brain evolution should be reframed  
240 within in a more inclusive proposition. We evidenced that a shared or conserved pattern of  
241 covariation could have an adaptive value or be instrumental to the emergence of derived modern  
242 humans functional capacities, rather than being considered a mere developmental or phylogenetic  
243 constraint<sup>21</sup>. In contrast, this study suggests that departure from an established pattern does not  
244 necessarily involve the presence of a modular behaviour and that high covariation may favour the  
245 emergence of functional specialisation, as predicted by the mosaic model.

246 In conclusion, we propose that the persistence of high levels of morphological covariation  
247 into adulthood in modern humans and Neanderthals is linked to the evolution of derived cognitive  
248 abilities. In addition, modern humans show high levels of integration between cortical areas  
249 throughout development. Unfortunately, the scarcity of immature Neanderthals with well-preserved  
250 skulls prohibits us from conclusively determining whether *H. neanderthalensis* brain followed the  
251 same developmental path as ours<sup>43,44</sup>. Yet, the strong covariation in adult brains shared by  
252 Neanderthals and *H. sapiens* only, suggests this is arguably the case.

253 Neural plasticity and innovative-explorative behaviours are typically associated with  
254 juvenile life stages, as well as the extension of childhood learning<sup>45,46</sup> and are at central to Mithen’s

255 theory of cognitive fluidity<sup>47,48</sup>, which postulates that only modern humans are capable of fully  
256 integrating diverse dominions of knowledge. Our evidence supports the argument that juvenilisation  
257 of the human (and possibly to some extent Neanderthal's as well) brain was driven by prolonged  
258 brain growth, mediated by the retention of unusually high degree of covariation between the  
259 different brain units into adulthood.

260

261

262

263

## 264 Methods

### 265 *Endocast segmentation*

266 Virtual endocasts of primate crania were generated from CT image stacks using a combination of  
267 Mimics 21.0 (Materialise, Ann Arbor, MI, USA) and Geomagic Studio 2014 (Research Triangle  
268 Park, NC). For each specimen, cranial bone was first segmented in Mimics with the gray-value  
269 range set conservatively to avoid extensive manual corrections later in the process. The endocranial  
270 cavity was then closed off at the foramen magnum using a flat plane spanning basion to opisthion.  
271 Next, a 3D object was generated, and all gaps below 1 mm in diameter were closed using the  
272 “*Wrap*” function before closing off all remaining openings (e.g., foramen ovale, optic canal) near  
273 the endocranial surface. This created a sealed cavity that was filled using the “*Cavity Fill*” tool.  
274 Endocasts were then imported as stereolithography (STL)-formatted surface files into Geomagic  
275 where excess material protruding through cranial foramina was removed and the polygon meshes  
276 were lightly smoothed using the “*QuickSmooth*” function. Endocast volumes were then measured in  
277 cubic centimeters (cm<sup>3</sup>) using the “*Compute Volume*” function.

278

### 279 *Automatic landmarking procedure*

280 The points on the template (*Piliocolobus badius*) were projected on all the other specimens using  
281 the function *placePatch()* from the R package ‘Morpho’<sup>49</sup>. In order to remove any incorrect  
282 projection the semi-landmarks on the curves were set bold-distanced using the function  
283 *pointsOnBezier()* from the ‘bezier’ R package<sup>50</sup> then the curves present on the sides of the endocast  
284 geometry were mirrored using the function *symmetrize()* from the R package ‘Morpho’. After this  
285 process was complete the semi-landmarks were slid along the curves by minimising the bending  
286 energy of a thin plate spine deformation (semi-landmarks relaxation) using the *slider3d()* function  
287 from the R package ‘Morpho’. This approach follows the algorithm described by Gunz et al.<sup>51</sup> and  
288 has been shown to be the most appropriate method to slide semi-landmarks on curves and surfaces  
289 according to Bookstein<sup>52</sup>.

290

### 291 *Shape analysis*

292 On each endocast (Supplementary Fig. 1), we manually digitised 21 anatomical and homologous  
293 landmarks, then performed a principal component analysis (PCA) to identify the individual closest  
294 to the consensus shape (*Piliocolobus badius* USNM 481795). We manually digitised 76 semi-  
295 landmarks placed equidistantly along curves and surfaces on the consensus specimen endocast and  
296 used it as the template individual (Supplementary Table 1). All landmarks were placed by using  
297 IDAV Landmark software. Once all the semi-landmarks were automatically placed, we imported  
298 the landmark coordinates into R version 4.0.1 for further analyses. We performed generalised  
299 Procrustes analysis (GPA) on all landmarks, implemented in the function *procSym* from the R  
300 package ‘Morpho’ to rotate, translate and scale landmark configurations to unit centroid size (CS),  
301 that is the square root of squared differences between landmark coordinates and centroid  
302 coordinates<sup>53</sup>. To visualise the multivariate ordination of the aligned Procrustes coordinates, we  
303 used a phylomorphospace using the first two regular non-phylogenetic PCA scores. We classified  
304 the species using similar taxonomic groups to those defined in Sansalone et al.<sup>4</sup> and Neaux et al.<sup>54</sup>:  
305 Hominoidea, Cercopithecinae, Colobinae, Platyrrhini, Strepsirrhini. Shape data have been

306 controlled for size (Extended Data Tables 2-3), sexual dimorphism effects and for measurement  
307 error.

308

### 309 *Phylogeny*

310 The phylogenetic tree used in our analyses is a time-calibrated tree based on a Bayesian estimate  
311 obtained from the 10kTrees Project v3<sup>55</sup> for the 146 extant species in our dataset. A maximum clade  
312 credibility tree of the extant species in the analysis was constructed from a set of 1000 molecular  
313 trees using the function MaxCredTree() from the R package ‘phangorn’<sup>56</sup>. Finally, the eight fossil  
314 species included in our dataset were manually added to the tree (available in Newick format in  
315 Supplementary Information) following the topological arrangement in refs.<sup>2,57,58</sup> using the RRphylo  
316 function *tree.merger*<sup>59</sup>. The full list of the accessed specimens is indicated in Supplementary Table  
317 2.

318

### 319 *Measurement error*

320 The measurement error associated with the digitisation of landmarks was measured on three  
321 replicates of 60 specimens representative of the total dataset variation. For each specimen we  
322 digitized only the homologous landmarks, subsequently we automatically applied the semi-  
323 landmarks following the procedure previously described. We calculated the mean Procrustes  
324 distances for each triplet of the same specimen occurring in the three replicas. We then computed  
325 the averages of all the mean values of the minimum and maximum values of each triplet. The  
326 amount of digitisation error, with respect to the total variation in the shape, can be expressed as a  
327 percentage. We calculated the ratio of the mean value for total digitisation and the mean of the total  
328 dataset. We found the digitization error in the endocast dataset was as low as 0.36% of the total  
329 variation, respectively. Because the measurement error was smaller than 5% in both datasets it  
330 could be safely assumed its effect on the results was negligible.

331

### 332 *Sexual dimorphism*

333 In order to account for the potential effect of sexual dimorphism on the shape data, we performed a  
334 Procrustes ANOVA to test for the presence of significant shape and size differences between males  
335 and females. The analysis returned a non-significant result ( $r^2 = 0.01$ ,  $p = 0.28$ ), suggesting that, at  
336 macroevolutionary scale, sexual dimorphism is not impacting the brain shape variation in Primates.  
337 Similar results were obtained when we tested for size differences between males and females ( $r^2 =$   
338  $0.01$ ,  $p = 0.24$ ).

339

### 340 *Size and phylogenetic correction*

341 The relationship between size (measured as CS; independent variable) and shape (measured as  
342 aligned Procrustes coordinates; dependent variable) was tested by means of multivariate  
343 regressions. We repeated all the following analyses by using residuals of the multivariate regression  
344 of shape vs size.

345 Specifically, to account for size effects on the ontogenetic series, we used shape residuals computed  
346 from separate, per developmental stage, multivariate regression. The shape residuals were used to  
347 perform size-free PLS analyses, and the results are summarised in Extended Data Table 2. Overall,  
348 we did not observe any difference from the pattern described by the standard version of the PLS.  
349 However, it must be noted the r-PLS were lower for each group. This is in agreement with previous  
350 findings reporting allometry and development as integrating factors, therefore the removal of the  
351 size component may reduce the observed levels of covariation<sup>60</sup>.

352 The same holds for the macroevolutionary analyses, which we repeated using residuals of  
353 multivariate regressions of shape vs size performed within a phylogenetic context using PGLS  
354 (Phylogenetic Generalised Least Squares) regression. Specifically, shape residuals have been  
355 computed using the function *PGLS\_fossil()* from the R package RRphylo. It must be noted that the  
356 PGLS analysis using shape as the respondent and size as the predictor variables and accounting for

357 phylogenetic variance covariance matrix, returned marginally significant results ( $p$ -value = 0.042;  $r^2$   
358 = 0.101) suggesting that size is explaining a relatively small fraction of the total shape variation,  
359 this result is in line with previous investigations evidencing a limited effect of size on primates'  
360 brain shape<sup>4,22</sup>.

361 We computed the Covariance Ratio (CR, see below for more details) values using shape residuals  
362 (results are summarized in Extended Data Table 3) for the different primate clades while accounting  
363 for phylogeny using the function *phylo.modularity()* from the R package geomorph. Furthermore,  
364 we used shape residuals to compute per-species CR values to then compute size-free evolutionary  
365 rates of covariation. Again, we did not notice any alteration in the pattern produced by the standard  
366 RRphylo analyses of evolutionary rates, with the major shifts identified on the same nodes.

367

### 368 *Assessing brain covariation*

369 We measured the magnitude of covariation between the different ontogenetic stages by employing  
370 the standard PLS analysis. PLS differs from linear regression by treating the two variables  
371 symmetrically rather than using one set of variables (independent) to predict the other. Instead, PLS  
372 constructs new variables that are linear combinations of the variables within each of the sets,  
373 accounting for as much as possible of the covariation between the two original sets of variables.  
374 The magnitude of morphological covariation in the brain at the macroevolutionary context has been  
375 assessed using the CR coefficient measured accounting for shared ancestry applying the function  
376 *phylo.modularity* from the R package 'geomorph'<sup>61</sup>. The CR coefficient is a measure of the overall  
377 covariation between modules divided by the overall covariation within modules. The CR coefficient  
378 ranges from 0 to positive values, where lower values indicate low covariation and high values  
379 indicate higher covariation, here departure from the null hypothesis of random association between  
380 modules is assessed via permutation. Furthermore, measuring the CR coefficient is insensitive to  
381 variation in sample size and number of variables as the variance of each module is not included.  
382 These analyses were repeated after accounting for the effect of size measured as logarithm of  
383 centroid size.

384 Finally, it has been recently noted<sup>62</sup> that sliding semi-landmarks using the minimum bending energy  
385 (BEN) approach may result in increased covariation between modules. Because we used semi-  
386 landmarks in our dataset, we repeated all the following integration analyses using shape coordinates  
387 derived using both the minimum BEN and minimum Procrustes distances (PRD) approaches to  
388 evaluate any potential discrepancy in the results. We found no significant discrepancies when using  
389 either sliding methods, hence we present only the results obtained from the analyses performed on  
390 the shape coordinates derived after using the minimum BEN approach.

391

### 392 *Assessing endocast modular partitioning*

393 Brain covariation was measured by dividing the brain into 6 distinct subunits following previously  
394 published protocols and on the recognition of traits on the cortical surface areas identified from the  
395 3D reconstruction<sup>2,4,23,35,63-65</sup> (see Supplementary Fig. 2).

396 1-2) The frontal and pre-frontal regions extend from the frontal pole anteriorly to the central sulcus  
397 posteriorly. The central sulcus is a longitudinal unfolding beginning on the medial surface of the  
398 brain. The frontal region borders with the postcentral gyrus of parietal lobe, and it is separated from  
399 the temporal lobe by the lateral sulcus<sup>66</sup>.

400 3) The anterior border of the parietal region is demarcated by the central sulcus and the inferior  
401 border is demarcated by the Sylvian fissure. It extends posteriorly where it meets the occipital areas.

402 4) The parietal lobe can be further subdivided into major subareas which can be identified from the  
403 endocranial surface (supramarginal gyrus, angular gyrus, intraparietal sulcus, superior parietal  
404 lobule)<sup>65</sup>.

405 5) The temporal lobe is separated from the other cortical area by the Sylvian fissure, a feature  
406 unique to primates<sup>67</sup>.

407 6) The occipital lobe is the most posterior region of the brain and borders the parieto-occipital  
408 fissure which separate it from the parietal areas<sup>68</sup>.

409 However, describing different modules on the endocasts can be challenging and to better define the  
410 different regions we accounted for the uncertainties of assessing clear boundaries between the  
411 different modules we applied two different strategies.

412 1) We defined four different modular configurations and evaluate between them by using the  
413 standardised test statistics based on the comparison of the Covariance Ratio (CR) measurement.  
414 This assesses the covariances within and among hypothesised modules and compares this ratio with  
415 a null hypothesis of random assignment of shape variables to partitions<sup>69,70</sup>. We found that the most  
416 supported configuration was the one formed by four distinct modules (Supplementary Fig. 2 and  
417 Supplementary Table 3).

418 2) We devised a novel strategy to measure the intensity of local modularity and integration without  
419 defining modules a priori. In geometric morphometrics applications, a module is defined as a  
420 discrete region characterised by greater integration internally than externally. To locate brain areas  
421 matching this condition, for each semilandmark we selected its 9 closest semilandmarks, forming a  
422 candidate modulet (N-Core) of 10 semilandmarks. All the other semilandmarks of the entire set  
423 define a second module (R-Core) (Extended Data Fig. 1). We calculated the Covariance Ratio (CR)  
424 between N-Core and R-Core, repeated the operation over all semilandmarks for the entire set and  
425 mapped CR values on a reference mesh. The CR between each N-Core and its corresponding R-  
426 Core indicated how much N-Core is likely to form a discrete module (see Supplementary Fig. 3-4).  
427 A similar procedure was used to calculate the local integration by computing the correlation of the  
428 first PLS axis between N-Cores and R-Cores. At each iteration, the Procrustes Generalised Analysis  
429 (GPA) is performed separately on each of the two blocks (N and R-Cores). This way, by using PLS  
430 the level of integration was calculated iteratively over all semilandmarks of the entire sample.

431

#### 432 *RRphylo and overfitRR*

433 We derived rates of brain shape evolution by the *RRphylo* method<sup>71</sup>, available within the R package  
434 ‘*RRphylo*’ (v.2.5.0). Under *RRphylo*, consequent phenotypic changes occurring along a phyletic  
435 line, from the root to a species are given by the equation  $\Delta P = \beta_1 l_1 + \beta_2 l_2 + \dots + \beta_n l_n$  where  $\beta_{ith}$  and  
436  $l_{ith}$  represent the regression coefficient and branch length, respectively, for each  $ith$  branch along the  
437 phyletic line. Being regression slopes, the  $\beta$  coefficients represent the magnitude of phenotypic  
438 change occurring along each branch, that is the actual rate of phenotypic evolution. The matrix  
439 solution to find the vector of  $\beta$  coefficients for all the branches is given by the equation  $\hat{\beta} =$   
440  $(L^T L + \lambda I)^{-1} L^T y$ ; where  $L$  is the matrix of species to root time distances of the tree (the branch  
441 lengths), having tips as rows,  $\hat{y}$  is the vector of species phenotypes, and  $\hat{\beta}$  is the vector of rates.  $\lambda$  is  
442 a penalisation factor which prevents overfitting by penalising extremely large rates. Lambda ( $\lambda$ ) is  
443 derived by means of maximum likelihood estimation by minimising rate variance within clades as  
444 compared to variance between clades.

445 To locate clade-wise shifts in evolutionary rates, we used the function *search.shift* from the package  
446 ‘*RRphylo*’<sup>71</sup>. *search.shift* is specifically meant to automatically scan the phylogeny to identify  
447 shifts in absolute phenotypic evolutionary rates. Given rates as produced by *RRphylo*, *search.shift*  
448 starts by selecting all the subclades within the tree ranging from one tenth to one half of the total  
449 tree size. For each clade, it computes the difference between the mean absolute rate pertaining the  
450 branches within the clade and the same figure for all other branches within the tree. Each difference  
451 is compared to a random distribution of 1,000 differences derived by randomly swapping rate  
452 values among the branches.

453 To account for sampling, phylogenetic uncertainty in tree topology and branch lengths, we used the  
454 *RRphylo* function *overfitRR*. Over 100 consecutive iterations, the function randomly removes a  
455 number of tips corresponding to 25% of the tree size and swaps species phylogenetic position of the  
456 10% of the remaining species. For instance, a topology of the kind ((A, B), C) might change to ((C,  
457 B), A) or ((A, C), B). In addition, the age of 10% of the tree nodes is changed ‘moving’ the node in



458 between the age of its direct ancestor and the age of its oldest daughter node. At each iteration,  
459 *overfitRR* performs *search.shift* on pruned tree and data testing whether the pattern found with the  
460 original data is robust to sampling and phylogenetic uncertainty issues. The results of the analysis of  
461 rates of CR evolution were confirmed after accounting for phylogenetic uncertainty, by randomly  
462 swapping tree branches and node ages, suggesting they are not a consequence of the tree topology  
463 we used (Hominoidea:  $p = 0.99$ ; Strepsirrhini:  $p = 0.01$ ; Cebidae:  $p = 0.01$ ).

464

465 **Data availability:** All data required to replicate this study are available at (definitive Figshare link)

466 **Code availability:** The code required to replicate this study is available at (definitive Figshare link)

467

468 **Acknowledgments:** We are grateful to Dr. Matt White, Dr. Paolo Piras and Dr. Carmelo Fruciano  
469 for their useful comments during manuscript preparation. We are grateful to Dr. Amélie Beaudet  
470 and two anonymous referees whose contributions greatly improved the quality of the manuscript.

471

472 **Author Contributions Statement:** The study was conceived by GS, AP, SW and PR. DRM, SL,  
473 AP, JL, MM and KA processed the endocasts. SL and GS digitized the landmarks. GS, PR, AP, CS,  
474 SC, MM and AM analyzed the data. GS, PR, AP and SW wrote the manuscript with significant  
475 contribution from all the other authors.

476

477 **Competing Interests Statement:** The authors declare no competing interests.

478

## 479 **Figure Captions**

480 **Figure 1.** Patterns of postnatal integration in modern humans and chimpanzees. **a.** Postnatal growth  
481 stages for *Homo sapiens*, *Pan troglodytes*, *Gorilla gorilla* (only stages 4 and adult) and r-PLS  
482 values per ontogenetic stage. The meshes in the lower left corner refer to the average for each stage  
483 and are coloured according to the magnitude of integration. **b.** Pairwise r-PLS values between brain  
484 modules in adult *H. sapiens*, *P. troglodytes* and *G. gorilla*. **c.** Comparison of r-PLS values per  
485 ontogenetic stage between *H. sapiens* and *P. troglodytes* calculated using the NR-PLS approach,  
486 that does not require the *a priori* definition of brain modules. Warm (cold) colours refer to low  
487 (high) magnitude of integration. Animal silhouettes were available under Public Domain license at  
488 phylopic (<http://phylopic.org/>). Specifically, *Homo sapiens* (<http://phylopic.org/image/c089caae-43ef-4e4e-bf26-973dd4cb65c5/>) - No Copyright - Public Domain Dedication 1.0; *Pan troglodytes*  
489 (<http://phylopic.org/image/2f7da8c8-897a-445e-b003-b3955ad08850/>) - credit to T. Michael  
490 Keeseey (vectorization) and Tony Hisgett (photography) - Creative Commons Attribution 3.0  
491 Unported license.

493

494 **Figure 2.** Macroevolution of primate brain morphology and covariation. **a.** PC1/PC2  
495 phylomorphospace of primate brain shape variation. **b.** Distribution of CR rate shifts on the tree.  
496 Magenta shades indicate a slowdown in CR rate of evolution, whereas the cyan shade indicates  
497 acceleration. Brain meshes represent the average shape for each clade and are coloured according to  
498 the magnitude of CR. Warmer colours refer to low CR values, cooler colours refer to high CR.

499

500 **Figure 3. a.** Distribution of CR evolutionary rates within hominoidea. The black vertical line  
501 represents the average rate of CR evolution calculated over the entire Primate tree, orange dots  
502 indicate internal nodes in the phylogeny. **b.** Evolutionary patterns of morphological integration  
503 within *Homo*. Magenta shades indicate a slowdown in the CR rate of evolution, the cyan shade

504 indicates acceleration. Brain meshes represent the average shape for *H. sapiens* plus *H.*  
505 *neanderthalensis* and all *Homo* species, respectively. The CR values are mapped over the endocast  
506 mesh. Warmer colours refer to low, cooler colours to high CR values.

507

## 508 **References**

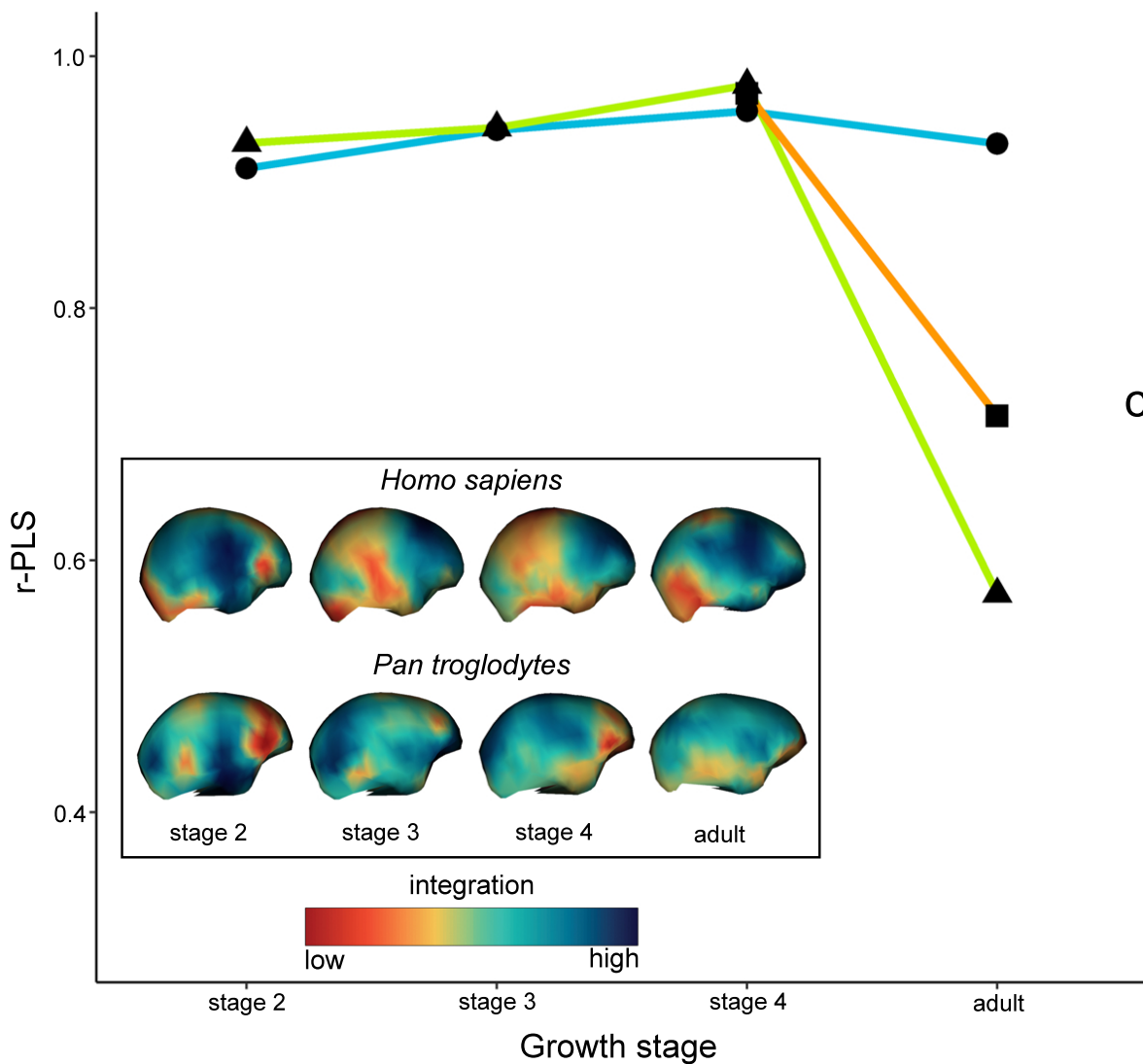
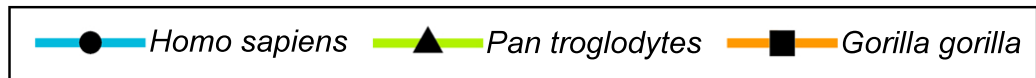
- 509 1. Ponce de León, M. S. *et al.* The primitive brain of early Homo. *Science* (80-. ). **372**, 165–171  
510 (2021).
- 511 2. Melchionna, M. *et al.* From Smart Apes to Human Brain Boxes. A Uniquely Derived Brain  
512 Shape in Late Hominins Clade. *Front. Earth Sci.* **8**, 273 (2020).
- 513 3. Du, A. *et al.* Pattern and process in hominin brain size evolution are scale-dependent. *Proc.*  
514 *R. Soc. B Biol. Sci.* **285**, 20172738 (2018).
- 515 4. Sansalone, G. *et al.* Variation in the strength of allometry drives rates of evolution in primate  
516 brain shape. *Proc. R. Soc. B Biol. Sci.* **287**, 20200807 (2020).
- 517 5. Gunz, P. *et al.* Neandertal Introgression Sheds Light on Modern Human Endocranial  
518 Globularity. *Curr. Biol.* **29**, 120-127.e5 (2019).
- 519 6. Finlay, B. L. & Darlington, R. B. Linked regularities in the development and evolution of  
520 mammalian brains. *Science* **268**, 1578–1584 (1995).
- 521 7. Barton, R. A. & Harvey, P. H. Mosaic evolution of brain structure in mammals. *Nature* **405**,  
522 1055–1058 (2000).
- 523 8. Harvey, P. H. & Krebs, J. R. Comparing Brains. *Science* (80-. ). **249**, 140–146 (1990).
- 524 9. Finlay, B. L., Darlington, R. B. & Nicastro, N. Developmental structure in brain evolution.  
525 *Behav. Brain Sci.* **24**, 263–278 (2001).
- 526 10. Barton, R. A. & Venditti, C. Human frontal lobes are not relatively large. *Proc. Natl. Acad.*  
527 *Sci. U. S. A.* **110**, 9001–9006 (2013).
- 528 11. Barton, R. A. & Venditti, C. Rapid evolution of the cerebellum in humans and other great  
529 apes. *Curr. Biol.* **24**, 2440–2444 (2014).
- 530 12. Sotiras, A. *et al.* Patterns of coordinated cortical remodeling during adolescence and their  
531 associations with functional specialization and evolutionary expansion. *Proc. Natl. Acad. Sci.*  
532 *U. S. A.* **114**, 3527–3532 (2017).
- 533 13. Gómez-Robles, A., Hopkins, W. D. & Sherwood, C. C. Modular structure facilitates mosaic  
534 evolution of the brain in chimpanzees and humans. *Nat. Commun.* **5**, 1–9 (2014).
- 535 14. Smaers, J. B. & Vanier, D. R. Brain size expansion in primates and humans is explained by a  
536 selective modular expansion of the cortico-cerebellar system. *Cortex* **118**, 292–305 (2019).
- 537 15. DeCasien, A. R. & Higham, J. P. Primate mosaic brain evolution reflects selection on  
538 sensory and cognitive specialization. *Nat. Ecol. Evol.* **3**, 1483–1493 (2019).
- 539 16. Montgomery, S. H., Mundy, N. I. & Barton, R. A. Brain evolution and development:  
540 Adaptation, allometry and constraint. *Proc. R. Soc. B Biol. Sci.* **283**, (2016).
- 541 17. Villmoare, B. Morphological Integration, Evolutionary Constraints, and Extinction: A  
542 Computer Simulation-Based Study. *Evol. Biol.* **40**, 76–83 (2013).
- 543 18. Goswami, A., Smaers, J. B., Soligo, C. & Polly, P. D. The macroevolutionary consequences  
544 of phenotypic integration: From development to deep time. *Philos. Trans. R. Soc. B Biol. Sci.*  
545 **369**, (2014).
- 546 19. Herculano-Houzel, S. The remarkable, yet not extraordinary, human brain as a scaled-up  
547 primate brain and its associated cost. *Proc. Natl. Acad. Sci. U. S. A.* **109**, 10661–10668  
548 (2012).
- 549 20. Barton, R. A. & Montgomery, S. H. Proportional versus relative size as metrics in human  
550 brain evolution. *Proc. Natl. Acad. Sci.* **116**, 3–4 (2019).
- 551 21. Avin, S., Currie, A. & Montgomery, S. H. An agent-based model clarifies the importance of  
552 functional and developmental integration in shaping brain evolution. *BMC Biol.* **19**, 97  
553 (2021).
- 554 22. Aristide, L. *et al.* Brain shape convergence in the adaptive radiation of New World monkeys.

- 555 *Proc. Natl. Acad. Sci. U. S. A.* **113**, 2158–2163 (2016).
- 556 23. Neubauer, S., Hublin, J.-J. & Gunz, P. The evolution of modern human brain shape. *Sci. Adv.*  
557 **4**, eaao5961 (2018).
- 558 24. Neubauer, S., Gunz, P., Scott, N. A., Hublin, J. J. & Mitteroecker, P. Evolution of brain  
559 lateralization: A shared hominid pattern of endocranial asymmetry is much more variable in  
560 humans than in great apes. *Sci. Adv.* **6**, 1–12 (2020).
- 561 25. Ni, X., Flynn, J. J., Wyss, A. R. & Zhang, C. Cranial endocast of a stem platyrrhine primate  
562 and ancestral brain conditions in anthropoids. *Sci. Adv.* **5**, 1–11 (2019).
- 563 26. Cobb, S. N. & O’Higgins, P. The ontogeny of sexual dimorphism in the facial skeleton of the  
564 African apes. *J. Hum. Evol.* **53**, 176–190 (2007).
- 565 27. Ragni, A. J. Trabecular architecture of the capitate and third metacarpal through ontogeny in  
566 chimpanzees (*Pan troglodytes*) and gorillas (*Gorilla gorilla*). *J. Hum. Evol.* **138**, 102702  
567 (2020).
- 568 28. Nadig, A. *et al.* Morphological integration of the human brain across adolescence and  
569 adulthood. *Proc. Natl. Acad. Sci. U. S. A.* **118**, e2023860118 (2021).
- 570 29. Ardesch, D. J. *et al.* Evolutionary expansion of connectivity between multimodal association  
571 areas in the human brain compared with chimpanzees. *Proc. Natl. Acad. Sci. U. S. A.* **116**,  
572 7101–7106 (2019).
- 573 30. Garin, C. M. *et al.* An evolutionary gap in primate default mode network organization. *Cell*  
574 *Rep.* **39**, 110669 (2022).
- 575 31. Watanabe, A., Balanoff, A. M., Gignac, P. M., Gold, M. E. L. & Norell, M. A. Novel  
576 neuroanatomical integration and scaling define avian brain shape evolution and development.  
577 *Elife* **10**, e68809 (2021).
- 578 32. Stout, D. & Chaminade, T. Stone tools, language and the brain in human evolution. *Philos.*  
579 *Trans. R. Soc. B Biol. Sci.* **367**, 75–87 (2012).
- 580 33. Bruner, E. & Iriki, A. Extending mind, visuospatial integration, and the evolution of the  
581 parietal lobes in the human genus. *Quat. Int.* **405**, 98–110 (2016).
- 582 34. Schaefer, N. K., Shapiro, B. & Green, R. E. An ancestral recombination graph of human,  
583 Neanderthal, and Denisovan genomes. *Sci. Adv.* **7**, 776–792 (2021).
- 584 35. Bruner, E., Spinapolice, E., Burke, A. & Overmann, K. A. Visuospatial Integration:  
585 Paleoanthropological and Archaeological Perspectives. in *Evolution of primate social*  
586 *cognition* 299–326 (Springer, 2018). doi:10.1007/978-3-319-93776-2\_19.
- 587 36. Bruner, E. & Gleeson, B. T. Body cognition and self-domestication in human evolution.  
588 *Front. Psychol.* **10**, 1111 (2019).
- 589 37. Porto, A., de Oliveira, F. B., Shirai, L. T., de Conto, V. & Marroig, G. The evolution of  
590 modularity in the mammalian skull I: Morphological integration patterns and magnitudes.  
591 *Evol. Biol.* **36**, 118–135 (2009).
- 592 38. Conde-Valverde, M. *et al.* Neanderthals and *Homo sapiens* had similar auditory and speech  
593 capacities. *Nat. Ecol. Evol.* **5**, 609–615 (2021).
- 594 39. Hardy, B. L. *et al.* Direct evidence of Neanderthal fibre technology and its cognitive and  
595 behavioral implications. *Sci. Rep.* **10**, 1–9 (2020).
- 596 40. Mondanaro, A. *et al.* A Major Change in Rate of Climate Niche Envelope Evolution during  
597 Hominid History. *iScience* **23**, 101693 (2020).
- 598 41. Leder, D. *et al.* A 51,000-year-old engraved bone reveals Neanderthals’ capacity for  
599 symbolic behaviour. *Nat. Ecol. Evol.* **2021** *59* **5**, 1273–1282 (2021).
- 600 42. Hublin, J. J., Neubauer, S. & Gunz, P. Brain ontogeny and life history in pleistocene  
601 hominins. *Philos. Trans. R. Soc. B Biol. Sci.* **370**, 20140062 (2015).
- 602 43. Gunz, P., Neubauer, S., Maureille, B. & Hublin, J. J. Brain development after birth differs  
603 between Neanderthals and modern humans. *Curr. Biol.* **20**, R921–R922 (2010).
- 604 44. Gunz, P. *et al.* A uniquely modern human pattern of endocranial development. Insights from  
605 a new cranial reconstruction of the Neanderthal newborn from Mezmaiskaya. *J. Hum. Evol.*

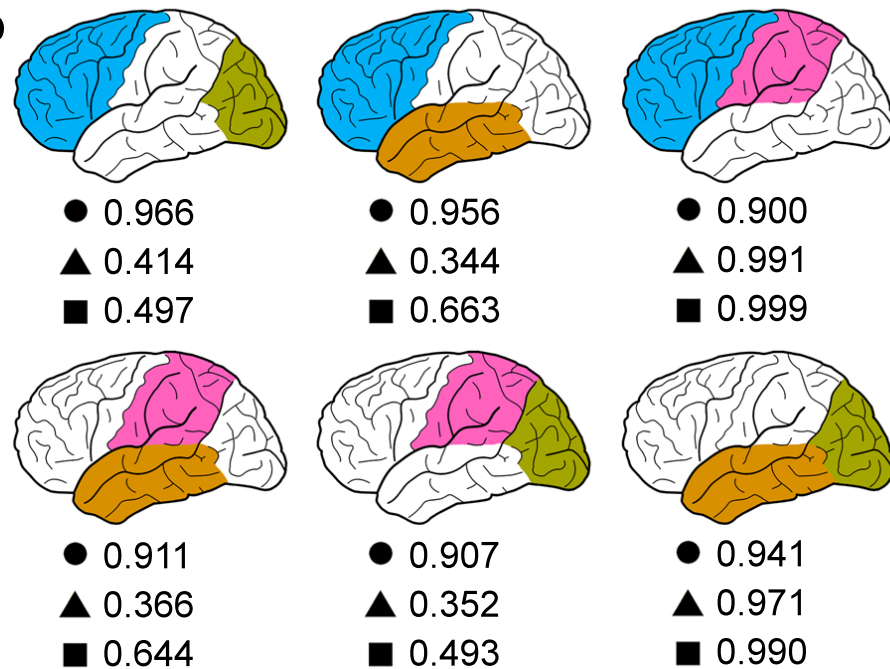
- 606 **62**, 300–313 (2012).
- 607 45. Gunz, P. *et al.* Australopithecus afarensis endocasts suggest ape-like brain organization and  
608 prolonged brain growth. *Sci. Adv.* **6**, eaaz4729 (2020).
- 609 46. Pellegrini, A. D., Dupuis, D. & Smith, P. K. Play in evolution and development. *Dev. Rev.*  
610 **27**, 261–276 (2007).
- 611 47. Mithen, S. The prehistory of the mind. *Cambridge Archaeol. J.* **7**, 269 (1997).
- 612 48. Mithen, S. *Creativity in human evolution and prehistory*. (Routledge, 2005).
- 613 49. Schlager, S. Morpho and Rvcg - Shape Analysis in R: R-Packages for Geometric  
614 Morphometrics, Shape Analysis and Surface Manipulations. in *Statistical Shape and*  
615 *Deformation Analysis: Methods, Implementation and Applications* 217–256 (2017).  
616 doi:10.1016/B978-0-12-810493-4.00011-0.
- 617 50. Olsen, A. bezier: Toolkit for Bezier Curves and Splines. (2018).
- 618 51. Gunz, P., Mitteroecker, P. & Bookstein, F. L. Semilandmarks in Three Dimensions. in  
619 *Modern Morphometrics in Physical Anthropology* 73–98 (Kluwer Academic Publishers-  
620 Plenum Publishers, 2006). doi:10.1007/0-387-27614-9\_3.
- 621 52. Bookstein, F. L. Integration, Disintegration, and Self-Similarity: Characterizing the Scales of  
622 Shape Variation in Landmark Data. *Evol. Biol.* **42**, 395–426 (2015).
- 623 53. Bookstein, F. L. Thin-plate splines and the atlas problem for biomedical images. in *Biennial*  
624 *International Conference on Information Processing in Medical Imaging* 326–342 (Springer,  
625 1991).
- 626 54. Neaux, D. *et al.* Basicranium and face: Assessing the impact of morphological integration on  
627 primate evolution. *J. Hum. Evol.* **118**, 43–55 (2018).
- 628 55. Arnold, C., Matthews, L. J. & Nunn, C. L. The 10kTrees website: a new online resource for  
629 primate phylogeny. *Evol. Anthropol. Issues, News, Rev.* **19**, 114–118 (2010).
- 630 56. Schliep, K. P. phangorn: phylogenetic analysis in R. *Bioinformatics* **27**, 592–593 (2011).
- 631 57. Dembo, M., Matzke, N. J., Mooers, A. Ø. & Collard, M. Bayesian analysis of a  
632 morphological supermatrix sheds light on controversial fossil hominin relationships. *Proc. R.*  
633 *Soc. B Biol. Sci.* **282**, 20150943 (2015).
- 634 58. Organ, C., Nunn, C. L., Machanda, Z. & Wrangham, R. W. Phylogenetic rate shifts in  
635 feeding time during the evolution of Homo. *Proc. Natl. Acad. Sci. U. S. A.* **108**, 14555–  
636 14559 (2011).
- 637 59. Castiglione, S., Serio, C., Mondanaro, A., Melchionna, M. & Raia, P. Fast production of  
638 large, time-calibrated, informal supertrees with tree.merger. *Palaeontology* **65**, e12588  
639 (2022).
- 640 60. Machado, F. A., Hubbe, A., Melo, D., Porto, A. & Marroig, G. Measuring the magnitude of  
641 morphological integration: The effect of differences in morphometric representations and the  
642 inclusion of size. *Evolution (N. Y.)*. **73**, 2518–2528 (2019).
- 643 61. Adams, D. C. & Otárola-Castillo, E. Geomorph: An r package for the collection and analysis  
644 of geometric morphometric shape data. *Methods Ecol. Evol.* **4**, 393–399 (2013).
- 645 62. Cardini, A. Integration and Modularity in Procrustes Shape Data: Is There a Risk of Spurious  
646 Results? *Evol. Biol.* **46**, 90–105 (2019).
- 647 63. Neubauer, S., Gunz, P. & Hublin, J. J. The pattern of endocranial ontogenetic shape changes  
648 in humans. *J. Anat.* **215**, 240–255 (2009).
- 649 64. Wild, H. M., Heckemann, R. A., Studholme, C. & Hammers, A. Gyri of the human parietal  
650 lobe: Volumes, spatial extents, automatic labelling, and probabilistic atlases. *PLoS One* **12**,  
651 (2017).
- 652 65. Pereira-Pedro, A. S., Bruner, E., Gunz, P. & Neubauer, S. A morphometric comparison of the  
653 parietal lobe in modern humans and Neanderthals. *J. Hum. Evol.* **142**, (2020).
- 654 66. Parks, A. N. & Smaers, J. B. The evolution of the frontal lobe in humans. in *Digital*  
655 *endocasts* 205–218 (Springer, 2018).
- 656 67. Preuss, T. M. Evolutionary specializations of primate brain systems. in *PRIMATE ORIGINS:*

- 657            *Adaptations and Evolution* 625–675 (Springer, 2007). doi:10.1007/978-0-387-33507-0\_18.  
658 68. Todorov, O. S. & de Sousa, A. A. Evolution of the occipital lobe. in *Digital Endocasts* 259–  
659 273 (Springer, 2018).  
660 69. Adams, D. C. & Collyer, M. L. Comparing the strength of modular signal, and evaluating  
661 alternative modular hypotheses, using covariance ratio effect sizes with morphometric data.  
662 *Evolution (N. Y.)*. **73**, 2352–2367 (2019).  
663 70. Adams, D. C. Evaluating modularity in morphometric data: Challenges with the RV  
664 coefficient and a new test measure. *Methods Ecol. Evol.* **7**, 565–572 (2016).  
665 71. Castiglione, S. *et al.* A new method for testing evolutionary rate variation and shifts in  
666 phenotypic evolution. *Methods Ecol. Evol.* **9**, 974–983 (2018).  
667

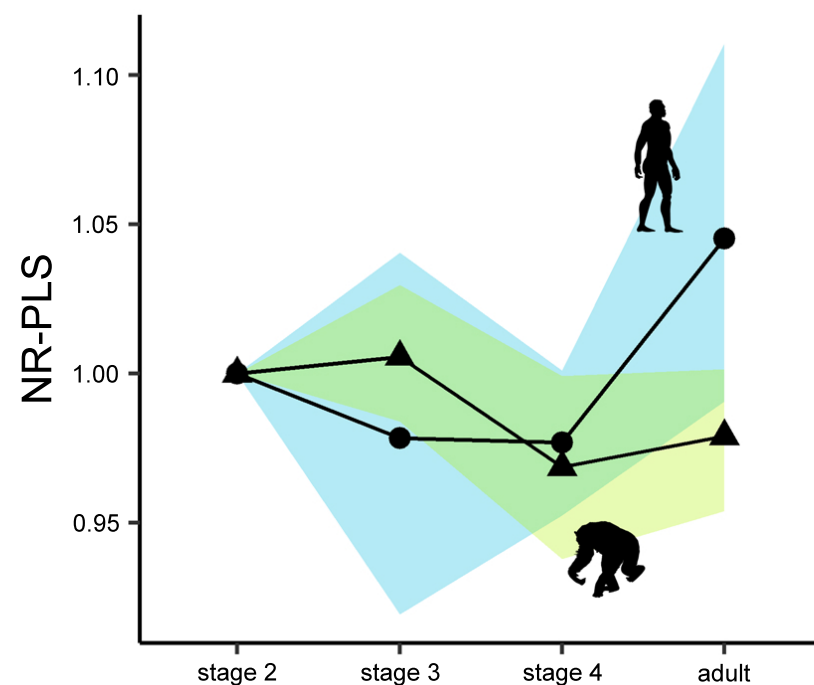
a

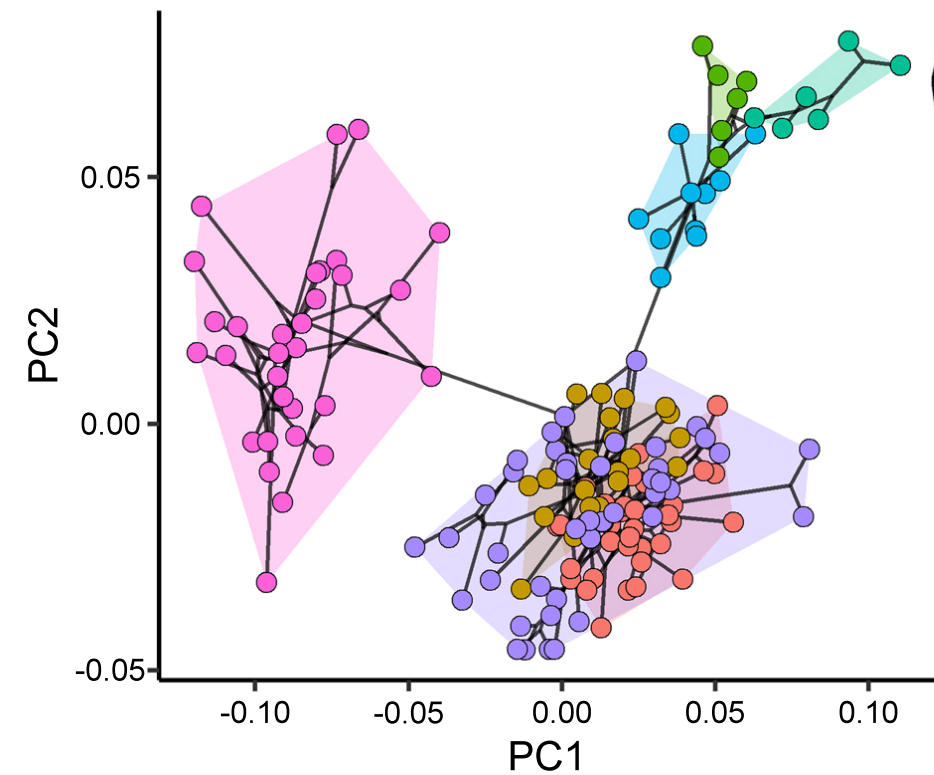
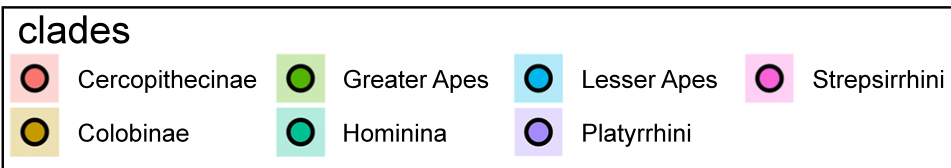
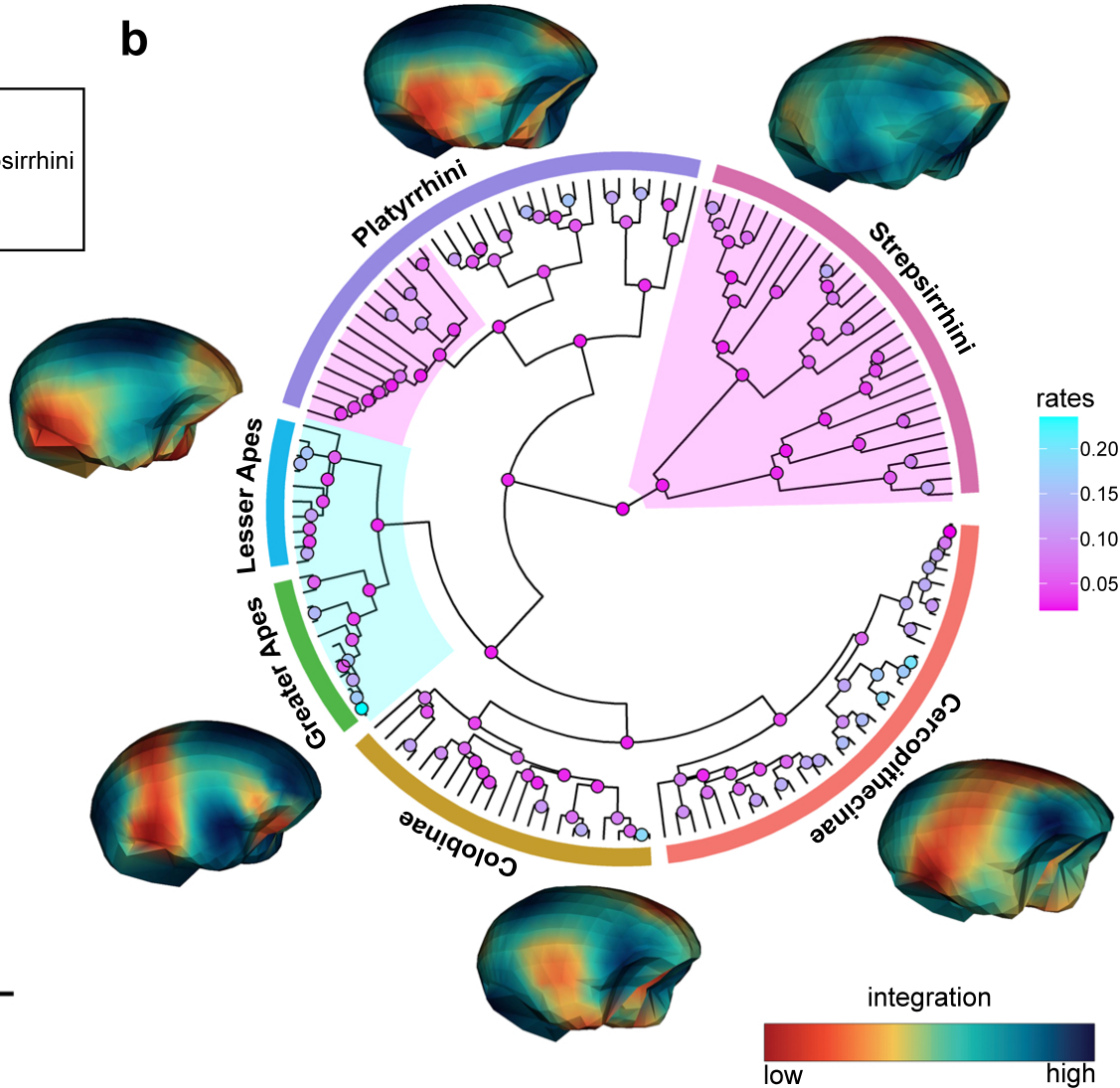


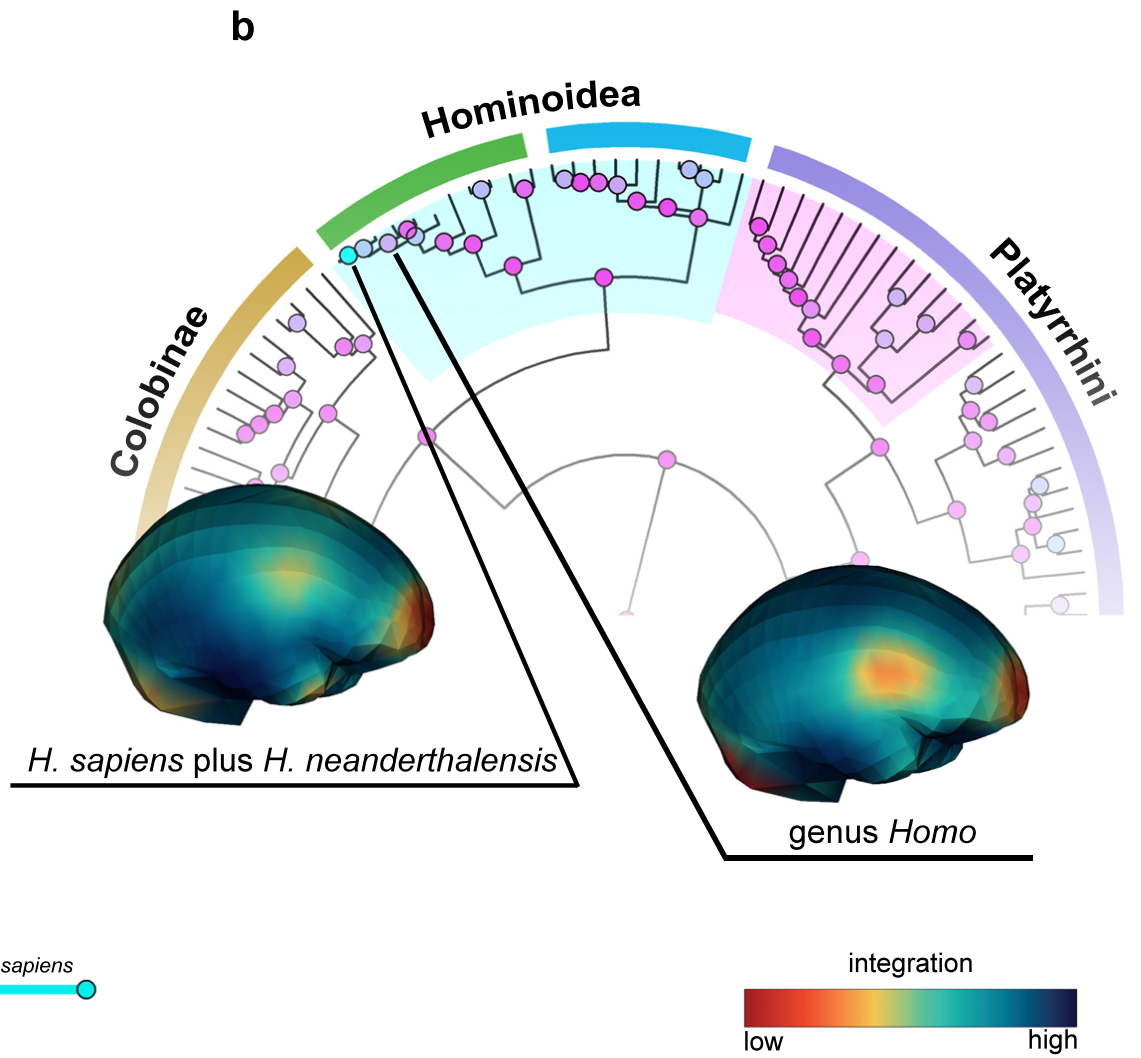
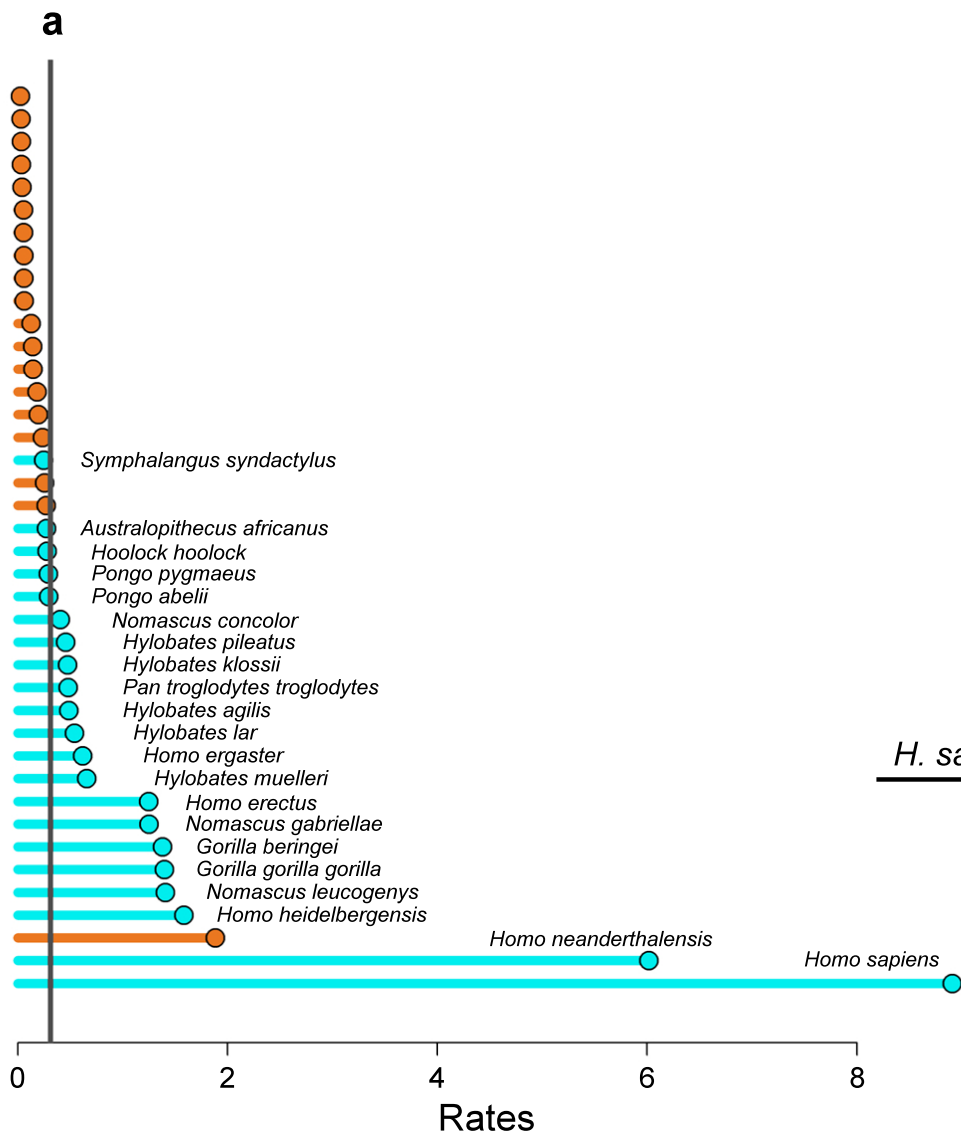
b



c



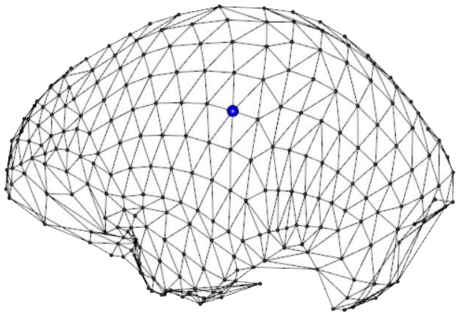
**a****b**





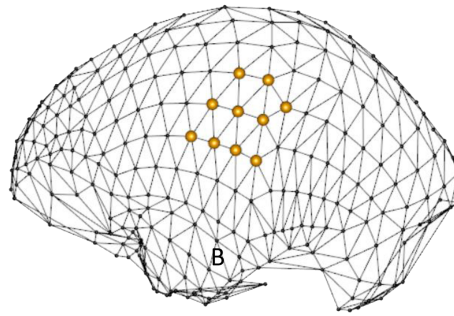
## Definition of N and R-Cores

**a**



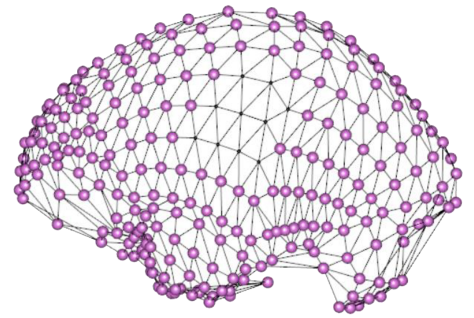
*i*-th semilandmark

**b**



N-Core

**c**



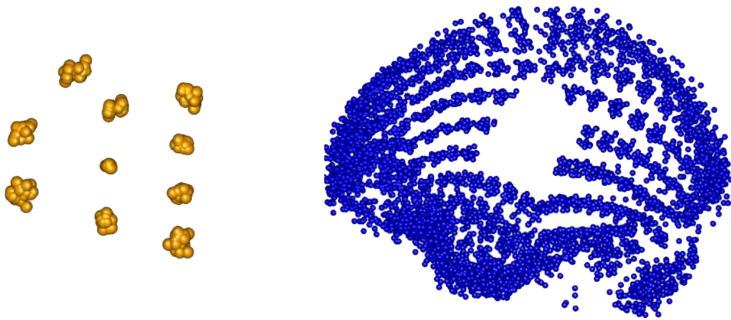
R-Core

**d**

GPA on N and R-Core



Partial Least Square (PLS)

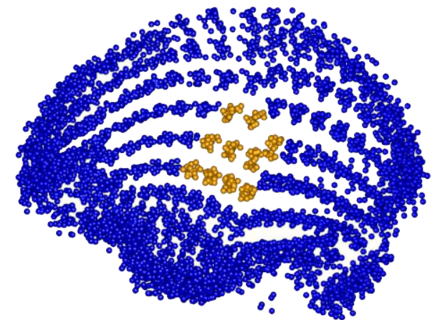


**e**

GPA on entire set

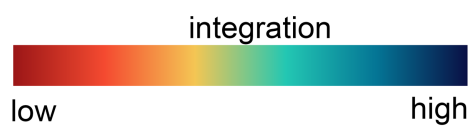
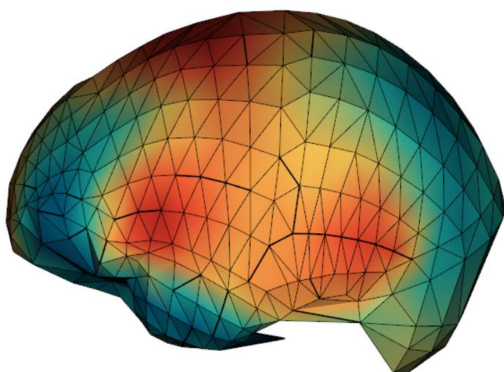


Covariance Ratio (CR)



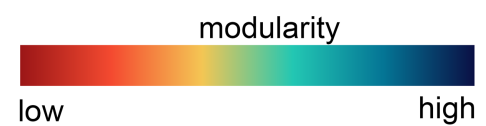
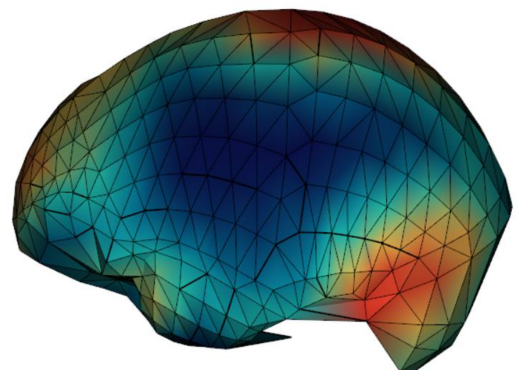
**f**

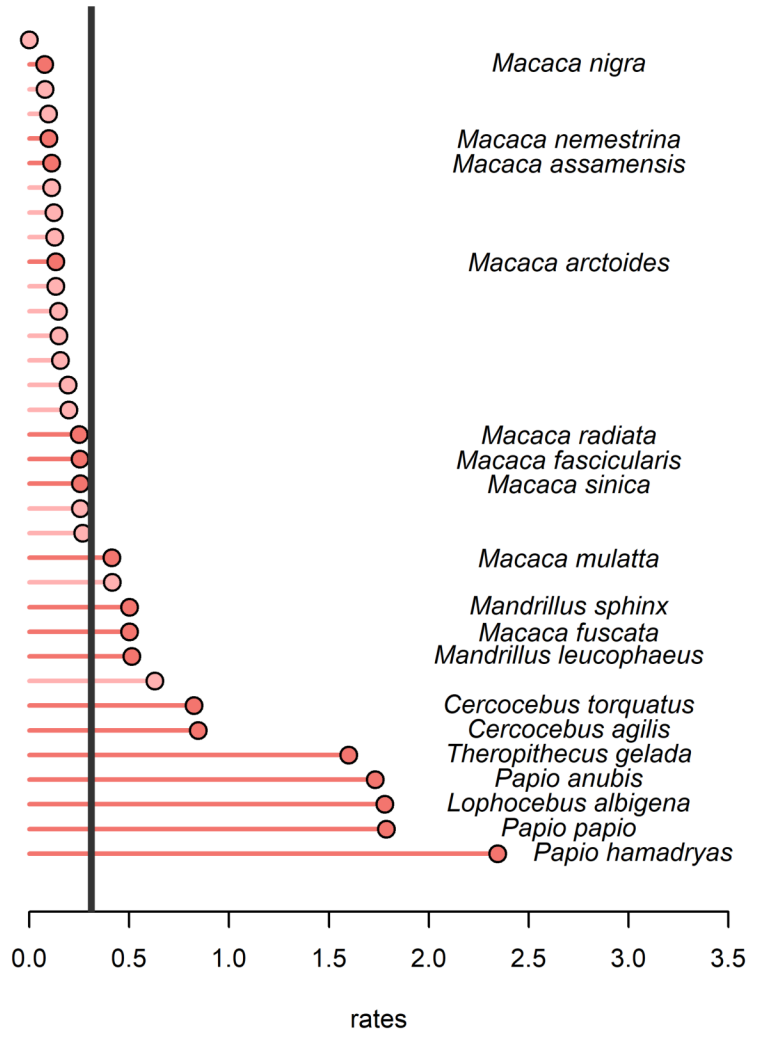
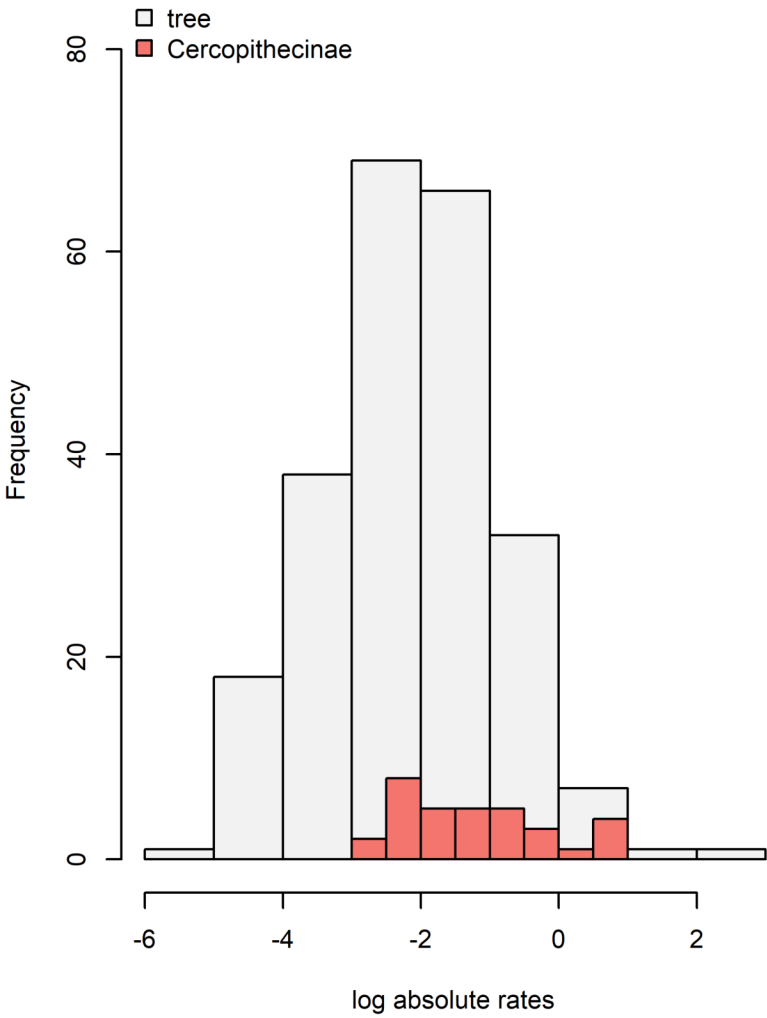
Map of Integration (PLS)

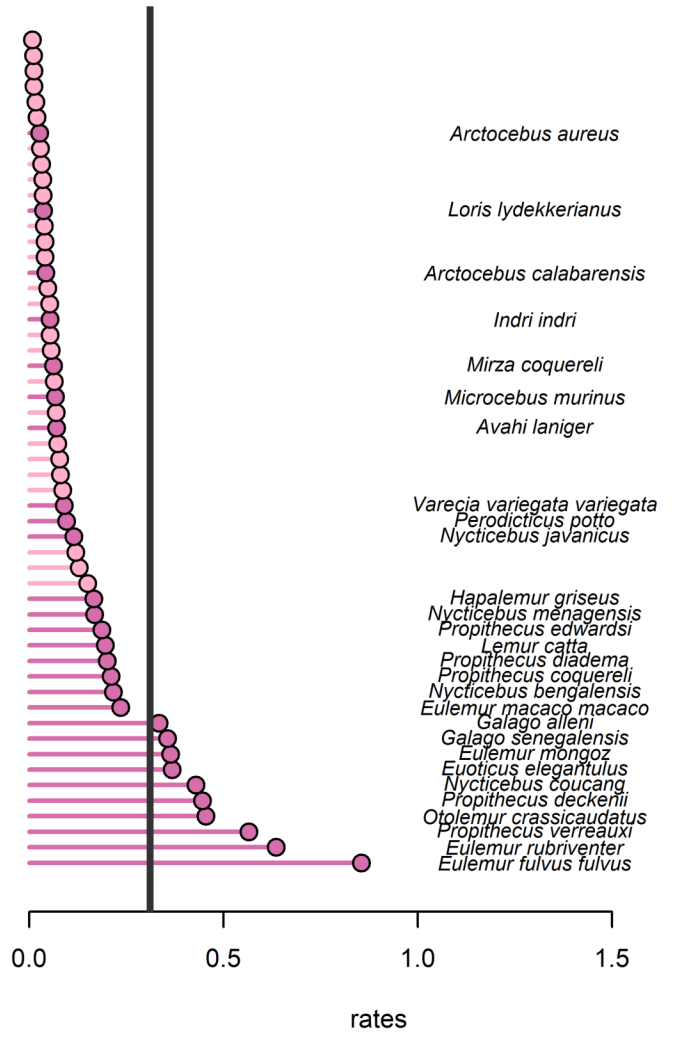
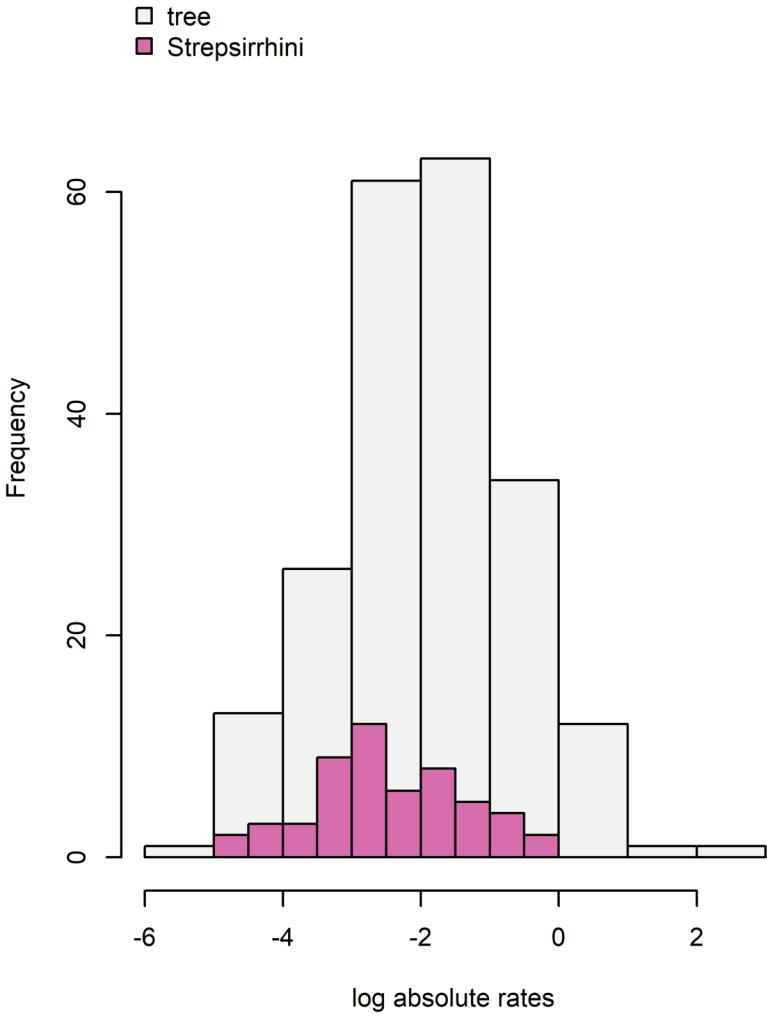


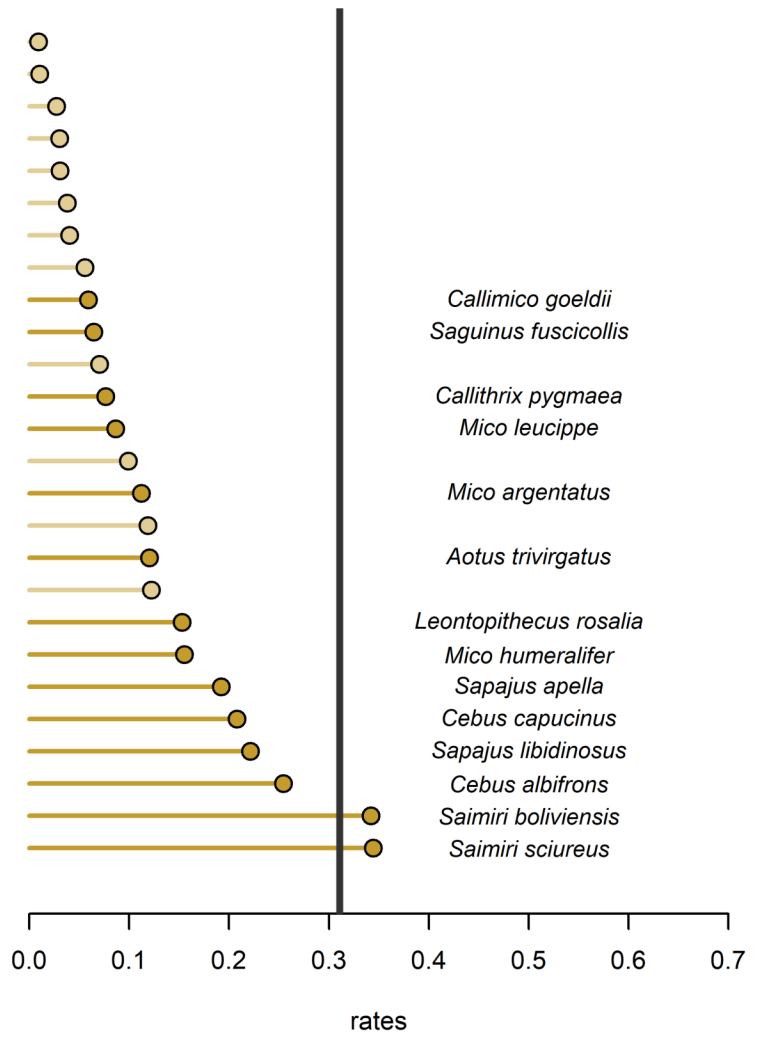
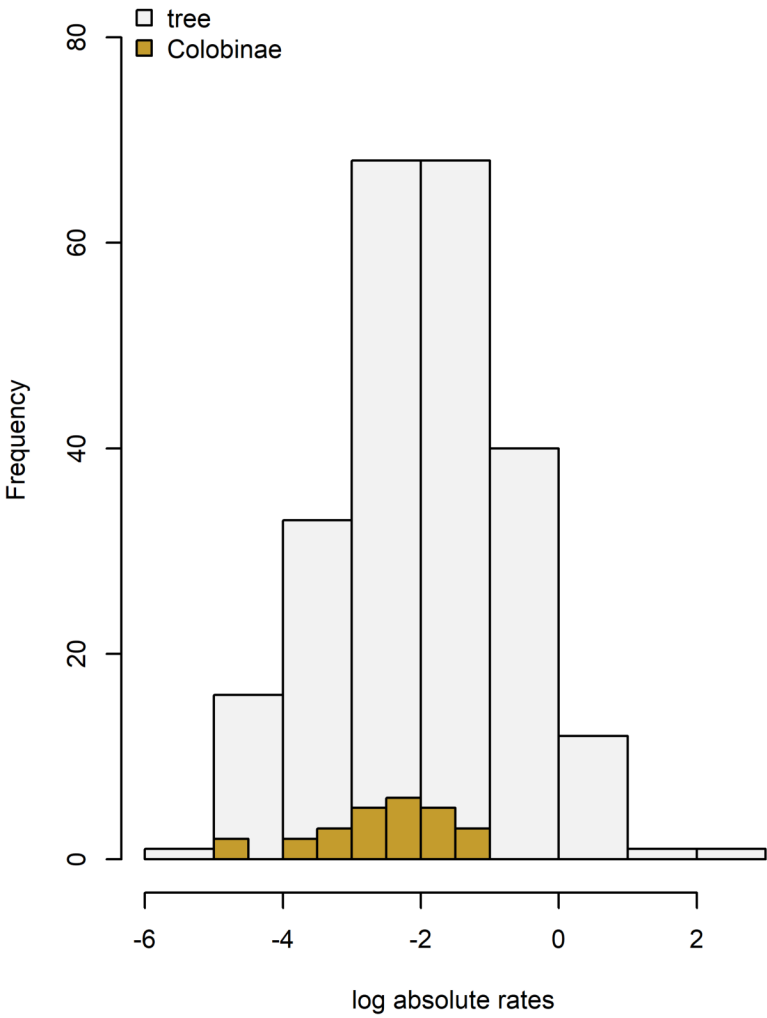
**g**

Map of modularity (CR)









<b>Taxon</b>	<b>Stage 2</b>	<b>Stage 3</b>	<b>Stage 4</b>	<b>Adult</b>
<i>Pan troglodytes</i>	0.93	0.94	0.97	0.57
<i>Homo sapiens</i>	0.91	0.94	0.96	0.93
			<b>Stages 3-4</b>	<b>Adult</b>
<i>Gorilla gorilla</i>			0.97	0.71
<i>Pongo sp.</i>			0.94	0.63

<b>Taxon</b>	<b>Stage 2</b>	<b>Stage 3</b>	<b>Stage 4</b>	<b>Adult</b>
<i>Pan troglodytes</i>	0.46	1.33	1.18	0.11
<i>Homo sapiens</i>	1.44	3.77	3.12	2.73
			<b>Stage 3-4</b>	<b>Adult</b>
<i>Gorilla gorilla</i>			0.73	0.21
<i>Pongo</i>			1.02	0.17

Clade	CR				
Hominoidea	0.963				
Cercopithecinae	0.825				
Colobinae	0.918				
Platyrrhini	0.767				
Strepsirrhini	0.726				

Pairwise test					
	Cercopithecinae	Colobinae	Hominoidea	Platyrrhini	Strepsirrhini
Cercopithecinae		0.468	<0.001	<0.001	<0.001
Colobinae			<0.001	<0.001	<0.001
Hominoidea				<0.001	<0.001
Platyrrhini					<0.001
Strepsirrhini					